Practical Aspects of 3D Heteronuclear NMR of Proteins

LEWIS E. KAY, DOMINIQUE MARION,* AND AD BAX

Laboratory of Chemical Physics, NIDDK, National Institutes of Health, Bethesda, Maryland 20892

Practical aspects regarding the acquisition and processing of 3D heteronuclear data sets are discussed, with particular emphasis on the 3D NOESY-HMQC experiment which combines the 2D NOE and the heteronuclear multiple-quantum coherence (HMQC) experiments. Slices through the 3D spectrum are equivalent to ^{15}N-filtered 2D NOESY spectra and exhibit sensitivity similar to that obtained in regular 2D NOE experiments. We discuss experimental procedures for obtaining maximum resolution with a relatively small number of t_1 and t_2 increments. In addition, a simple and efficient procedure for performing the third Fourier transformation that permits use of standard 2D software for processing in the other dimensions is described. Other important aspects of the data processing concern optimal digital filtering, noninteractive phasing, and minimization of the space needed for the processed data. © 1989 Academic Press, Inc.

Recently a number of groups have reported the use of three-dimensional NMR techniques for the simplification of complex spectra (*1–8*). For example, homonuclear (^1H) 3D techniques, combining *J* connectivity and NOE information, have been applied to a number of protein systems, clearly demonstrating the applicability of such techniques (*5, 7*). However, there is a fundamental limitation associated with the application of homonuclear techniques to the study of increasingly larger proteins: Proton magnetization decays rapidly in the time required for the scalar transfer of magnetization between spins, necessary for the labeling of the magnetization. In this regard, heteronuclear 3D techniques can be much more sensitive (provided that isotopic enrichment is used) since the transfer of magnetization between the heteronucleus and a directly coupled proton proceeds via a scalar coupling which is much larger than typical ^1H linewidths (*6, 8*). Also, the number of resonances in the heteronuclear 3D experiment is similar to that for two-dimensional NMR spectra; in contrast, the number of resonances in homonuclear 3D spectra is much larger. The relatively high sensitivity and the reduction in spectral overlap make the heteronuclear 3D experiment ideally suited for the study of proteins that are too large for detailed studies with the conventional 2D approach. Heteronuclear 3D experiments that separate conventional 2D spectra such as NOESY (*9, 10*), TOCSY/HOHAHA (*11, 12*), or COSY (*13–15*) according to the ^{15}N chemical shift of the amide nitrogen are particularly useful because of the relatively large ^{15}N chemical-shift dispersion (*16*).

Heteronuclear 3D NMR techniques require isotopic labeling of the system to be studied. For proteins this may be easily achieved by addition of suitably labeled nutri-

* On leave from Centre de Biophysique Moleculaire, Centre National de la Recherche Scientifique, 45071 Orleans Cedex 2, France.
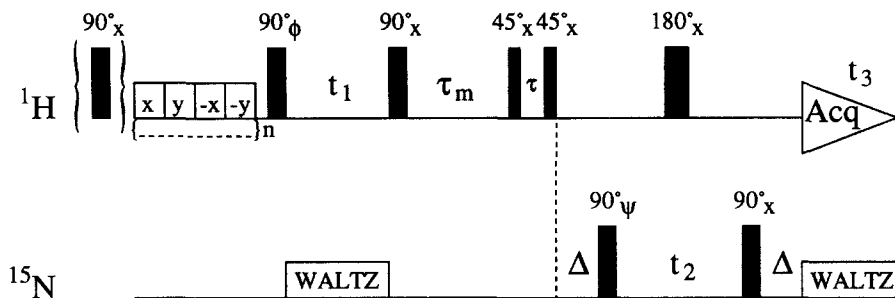
72

FIG. 1. Pulse scheme of the 3D NOESY-HMQC experiment. The ^{1}H carrier is positioned in the center of the amide region, and a DANTE type presaturation of water is used (*31*). The phase cycling used is as follows: $\phi = x, y, -x, -y$; $\psi = 4(x), 4(-x)$; Acq. $= 2(x), 4(-x), 2(x)$, with data for odd and even numbered scans stored separately. The entire sequence is repeated with ψ incremented by 90° to obtain complex data in the F_2 dimension. The first ^{1}H pulse is applied only for the first scan of each new t_1 increment and serves to establish a steady state of magnetization. Δ is set to a value slightly less than $1/2J_{NH}$ (4.5 ms) to minimize relaxation losses. The delay τ is carefully adjusted to maximize water suppression ($\tau \approx 1/(2\delta_{H_2O})$), where δ_{H_2O} is the offset of water. Depending on the spectrometer convention, the phases of the off-resonance presaturation pulses may have to be $(x, -y, -x, y)$ or $(x, y, -x, -y)$.

ents to the growth medium of microorganisms that contain the expression system for the molecule of interest (*16, 17*).

In a recent communication (*8*), we reported on the application of a NOESY-heteronuclear multiple-quantum coherence (NOESY-HMQC) 3D experiment to the protein staphylococcal nuclease (S. Nase). The final 3D spectrum obtained from this experiment displays NOE information between amide protons (F_3) and other protons in the protein (F_1) that are in close spatial proximity to the amide protons. The 3D spectrum is a collection of 2D (F_1–F_3) NOE maps separated in the F_2 dimension according to the ^{15}N chemical shift of the corresponding amide nitrogen. In addition to providing information necessary for sequential assignment of the backbone resonances (NH, CαH), the spectrum provides many of the distance constraints necessary for a structure determination.

As will be discussed below, high-quality heteronuclear 3D spectra can be recorded on samples of relatively low concentration (1–2 mM). In this paper the experimental aspects of the NOESY-HMQC pulse scheme will be discussed first, followed by an outline of several important practical considerations for the minimization of both data storage requirements and measuring time. Finally, a very effective and simple new strategy for the processing of 3D data will be presented, largely using existing 2D processing software.

THE NOESY-HMQC PULSE SCHEME

Figure 1 shows the NOESY-HMQC pulse sequence used in our laboratory. In the discussion that follows the convention of Griesinger et al. (*2, 3*) will be used, whereby the detection period is called t_3 and the two preceding evolution periods are referred to as t_1 and t_2. The variables t_1 and t_3 represent the "regular" time variables in the NOESY experiment and t_2 and t_3 are the "regular" time variables in the HMQC experiment. As in the NOESY experiment, ^{1}H magnetization excited by application

of the ^{1}H 90_ϕ° pulse is chemical-shift labeled during t_1 and is transferred during the mixing time (τ_m) to all spins in close spatial proximity. ^{15}N decoupling is employed during t_1 to remove heteronuclear scalar couplings. A homospoil pulse is applied in the middle of the mixing time to minimize coherent transfer of magnetization between scalar-coupled spins (18). For reasons to be discussed later, the carrier is positioned in the center of the amide proton region, and to obtain coherent presaturation of the H_2O resonance (19) a novel DANTE-type sequence is used. An analysis of this scheme is presented in the Appendix. Only a very weak presaturating RF field (10–15 Hz) is used, providing attenuation of the intense H_2O resonance by about a factor of 20, and saturating only a very narrow band of CαH resonances (<0.1 ppm) that are very close to the H_2O frequency. After the NOE mixing time, τ_m, the application of an off-resonance jump-and-return read pulse, 45_x°–τ–45_x°, generates transverse ^{1}H magnetization. The delay τ is adjusted to minimize excitation of water magnetization that has recovered during the mixing time or escaped saturation ($\tau \approx 1/(2\delta_{H_2O})$). The small amount of spurious transverse H_2O magnetization generated by the carefully calibrated 180° pulse at the midpoint of the t_2 period does not present any dynamic range problems and is removed from the 2D spectrum by the ^{15}N filtering effect of the HMQC sequence. The sequence that follows the NOE mixing period is similar to the regular ^{1}H–^{15}N HMQC shift correlation scheme (20, 21) (sometimes named forbidden echo (16)), and with phase cycling of the first 90° ^{15}N pulse, only signals from protons directly attached to ^{15}N remain during the detection period, t_3. For every t_2 value, a 2D data set is obtained with only amide protons in the detected (F_3) dimension and all protons in close spatial proximity to the amide protons in the F_1 dimension. The intensity of an H–NH cross peak in such a 2D spectrum is modulated as a function of t_2 by the ^{15}N chemical shift, and Fourier transformation with respect to t_2 of the (F_1, t_2, F_3) spectra results in the final 3D spectrum. For reasons to be discussed later, the Fourier transformations are executed in a different order.

At first sight, it may appear undesirable to record only the NH protons in F_3 and all protons in the F_1 dimension because this requires a larger minimum number of experiments to obtain sufficient digitization. Indeed, Fesik and Zuiderweg have recorded a 3D spectrum of a tripeptide dissolved in a deuterated solvent using an HMQC-NOESY 3D scheme (6), instead of a NOESY-HMQC scheme (8). In the former sequence, the NH proton shifts are recorded in the F_2 dimension. Note however, that the sensitivity of the experiment (given identical total measuring times) is essentially independent of this choice (22). Our choice for the scheme of Fig. 1 is based on the necessity to observe the crucial NH–Hα connectivities that otherwise would be buried in the wings of the intense H_2O resonance. At the low concentrations used (1–2 mM) typically a width of at least 0.7 ppm centered about the water is unobservable in the (F_1, F_2) = (NH, CαH) region of 2D NOESY spectra.

Since only NH resonances are detected during t_3, it is desirable to position the carrier at the center of the NH region. This minimizes the size of the data matrix that needs to be recorded.

Because of the large number of (t_1, t_2) experiments needed for a 3D spectrum with sufficient digital resolution, only a limited number of scans can be acquired for every (t_1, t_2) value. Therefore, only a relatively short phase cycle can be utilized. In practice, we find it sufficient to use a 16-step cycle, incrementing the phase of ϕ in 90° steps to
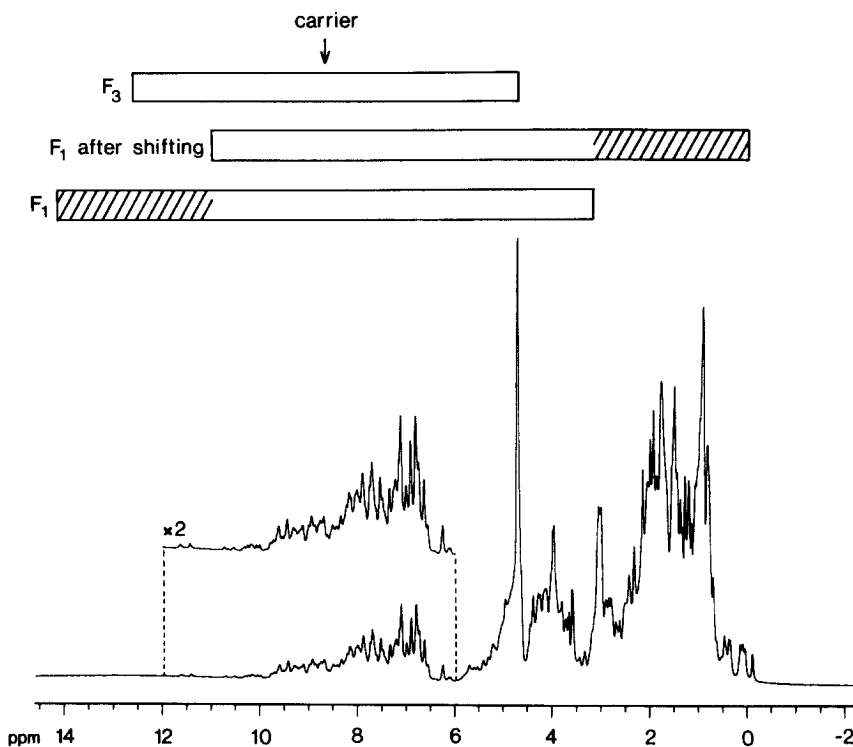
FIG. 2. Spectrum of S. Nase indicating the positioning of the ^{1}H carrier for recording the 3D experiment. The spectral windows employed in F_1 and F_3 are indicated in the top of the figure. Using either an acquisition (real or complex data in t_1) or a processing procedure (complex data in t_1) the carrier position is shifted in the F_1 dimension and an unfolded spectrum can be obtained. This is illustrated by the middle spectral window where the hatched region indicates the portion of the window that has been shifted.

obtain complex data in the F_1 dimension and to suppress axial peaks at $F_1 = 0$; the phase ψ is incremented in 90° steps to obtain quadrature information in the F_2 dimension and to eliminate signals during t_3 from protons not attached to ^{15}N. Because of the small number of scans per (t_1, t_2) value, the use of dummy scans to establish a steady state of magnetization prior to each new (t_1, t_2) value is undesirable.[1] Instead, we use a single 90° pulse (Fig. 1) prior to the start of each new (t_1, t_2) experiment.

PRACTICAL CONSIDERATIONS FOR MAXIMIZING F_1 AND F_2 RESOLUTION

Figure 2 illustrates the regular 1D spectrum of S. Nase with the carrier positioned in the center of the NH region. At first glance, it might appear that with the carrier in this position, a very large spectral window would be required in the F_1 dimension since resonances showing NOE connectivities to the NH protons lie in all regions of

---

[1] The number of dummy scans required and hence the actual savings in acquisition time is highly dependent on the dead time between each experiment (i.e., the time spent in disk I/O transfers and reloading of the pulse programmer) and varies for different types of spectrometers.

the 1D spectrum. A large spectral window would, of course, result in the need to acquire a large number of t_1 increments for sufficient resolution. In fact the F_1 spectral window that we employ is much smaller than might be anticipated and is indicated by the window marked F_1 in the figure. Use of this smaller spectral window is possible without introducing confusing folding artifacts by employing one of two different procedures depending on whether real data, acquired by TPPI (23), or complex data, acquired by the method of States et al. (24), are obtained in t_1.

For the TPPI case, the phase of the proton pulse immediately preceding the t_1 period can be incremented by $\pi/4$ for successive t_1 increments, instead of the usual $\pi/2$ increment.[2] Incrementing the phase by $\pi/2$ decreases the measured precession frequencies of all spins by SW/2 Hz (SW, spectral width) relative to the carrier, such that after a real Fourier transformation no folding is obtained for resonances that are within $\pm$SW/2 of the carrier. By incrementing the phase by $\pi/4$ the precessional frequencies are decreased by SW/4 Hz (instead of SW/2 for regular TPPI), and resonances between SW/4 and -3SW/4 Hz of the carrier are not folded. In other words, by incrementing the phase of the first ^{1}H pulse by $\pi/4$ the carrier is effectively moved downfield by SW/4 and folding of the data does not occur. In this way spectra can be acquired in which the position of the carrier need not be fixed from one ^{1}H dimension to the next.

If complex data are acquired in t_1 (using the method of States et al.) the precessional frequencies of all signals must be increased by SW/4 so that the carrier is positioned in the center of the spectrum prior to Fourier transformation of the data. This can be achieved using a procedure analogous to that discussed for TPPI data acquisition with the exception that the phase of the acquired signal must now be shifted by $-\pi/2$ for each t_1 increment.[2] Note that the sign of this phase shift is opposite to that required for real data since the carrier must be shifted in the opposite direction. In addition, the magnitude of the phase shift is doubled since for complex data the phase shift per data point is twice as large as for real data. Alternatively, shifting the carrier upfield can be performed during the data processing stage by multiplication of the time domain data $S(t_1, t_2, t_3)$ by $\exp\{i\pi t_1/(2\Delta t_1)\}$, where Δt_1 is the t_1 increment value. Such multiplication can conveniently be accomplished by using the routine that normally is used for the linearly frequency-dependent phase correction of frequency-domain data ($20, 25, 26$).

In the ^{15}N dimension (F_2), the carrier is positioned near the center of the amide region. Folding of a few resonances near the outer edges of the ^{15}N chemical-shift region can be used in the 3D experiment provided that a 2D ^{1}H–^{15}N correlation map with a sufficiently large ^{15}N spectral width is initially recorded. If the first t_2 increment (including the 180° ^{1}H pulse plus $4/\pi$ times the 90° ^{15}N pulse, as will be discussed in the processing section) is set to $\Delta t_2/2$, the linear phase correction will be 180°, and the folded resonances will appear with opposite phase relative to the unfolded resonances (provided that complex data are acquired in the t_2 dimension) making them easily identified. Use of extensive folding in the F_2 dimension may lead to signal cancellation of resonances with opposite sign and therefore should be avoided. As mentioned

---

[2] Depending on the convention of the spectrometer, the sign of the phase increment may have to be reversed.
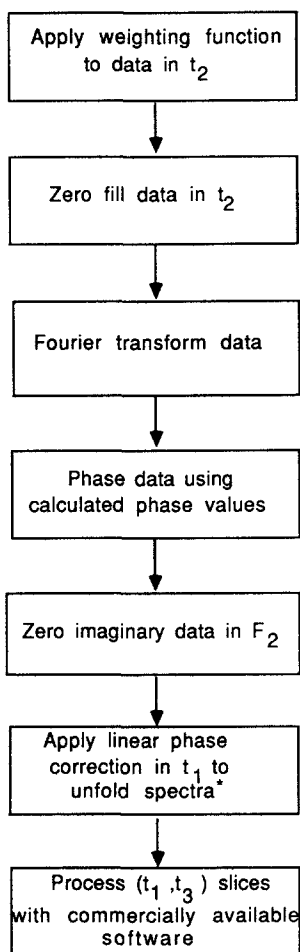
FIG. 3. Flowchart indicating the steps taken in processing the 3D data matrix. *If complex t_1 data were recorded.

before, the amide ^{15}N resonances show a substantial chemical-shift dispersion (≈ 35 ppm). However, because of the low magnetogyric ratio of ^{15}N, the spectral width required in the ^{15}N dimension is relatively small, and only a modest number of t_2 increments is needed for a t_2 acquisition time on the order of T_2. Longer t_2 acquisition times would result in poorer sensitivity per unit of measuring time.

We have recorded 3D experiments on our Bruker-AM and Nicolet-NT spectrometers as sets of 2D experiments, using standard 2D pulse programming procedures. The t_2 delay is incremented after acquisition of each 2D data set is completed.

PROCESSING STRATEGY

Figure 3 shows a block diagram of the steps involved in the processing of the 3D data set. As mentioned above, the data for each t_2 value are acquired and stored as

separate 2D data sets. For each t_2 value, two 2D data sets are acquired, corresponding to the real ($\psi = x, -x$) and the imaginary ($\psi = y, -y$) data in the t_2 dimension. The processing strategy that we use considers the data as a set of $2N$ 2D (t_1, t_3) NOESY matrices, where N is the number of complex t_2 points. To this end, the data are first processed in the t_2 (^{15}N) dimension, using simple software routines to be discussed later. The t_2 Fourier transformation is performed efficiently, without changing the data structure by transposition routines. This facilitates the use of any commercially available software for the subsequent transformations in t_1 and t_3. The software developed for processing in the t_2 dimension is written in modular form, with all manipulations that would normally be applied to each point in a one-dimensional process now applied to each (t_1, t_3) 2D matrix. The software is written for complex t_2 data, although, with a straightforward modification, real data can be processed as well.

The first steps in processing of the data in the t_2 dimension are the application of a weighting function and zero-filling. In the t_2 dimension, we typically use a doubly phase shifted sine-bell window function, shifted by about 60° at the beginning of the window and by about 10° at the end. The phase shift at the end of the sine bell is used to avoid too low a weighting factor for the last t_2 increments, improving sensitivity and resolution slightly, at the expense of a small (in practice not noticeable) increase in truncation artifacts in the F_2 dimension. Zero-filling in the F_2 dimension is essential; doubling the length of the time-domain data by adding zeroes to the end of the time domain is sufficient for providing adequate digitization in the frequency domain.

Fourier transformation in the t_2 dimension is accomplished using a modified version of a one-dimensional fast Fourier transform routine (FFT) which calculates the discrete complex Fourier transform of a set of N points, where N is a power of 2 (27). Figure 4 illustrates the manipulations that must be performed on the (t_1, t_3) planes in carrying out a t_2 transform. The FFT routine that we employ consists of two distinct parts: the bit reversal routine and the Danielson-Lanczos (butterfly) algorithm. During the first step, each (t_1, t_3) plane is reshuffled according to the prescription given for each point in the 1D transform. Because of the convenient storage of each (t_1, t_3) plane as an individual file this only amounts to a renaming of the planes (without the lengthy process of physically moving the data). This is indicated schematically in Fig. 4 where the labels of the two planes highlighted are interchanged with their relative positions in the data matrix remaining fixed. When points N_k and N_m are combined in the subsequent section of the 1D transform (butterfly algorithm), the equivalent combination of all points in planes corresponding to the points N_k and N_m in t_2 must be performed. A detailed description of the mechanics of the discrete 1D Fourier transform is provided in reference (27). Upon completion of the Fourier transformation, a (t_1, F_2, t_3) matrix is obtained with the zero frequency at one end of the spectrum. The data are reshuffled so that the carrier frequency is placed in the middle of the spectrum with positive and negative frequencies to the left and right of the carrier, respectively, in accord with NMR convention.

After Fourier transformation, the data are phased using a noninteractive phasing procedure (28). To a good approximation, the first 90° ^{15}N pulse can be replaced by a δ pulse followed by a delay of $2\tau_{90°}(^{15}N)/\pi$, where $\tau_{90°}(^{15}N)$ is the duration of the 90° ^{15}N pulse. Similarly, the final 90° ^{15}N pulse may be replaced by a δ pulse preceded
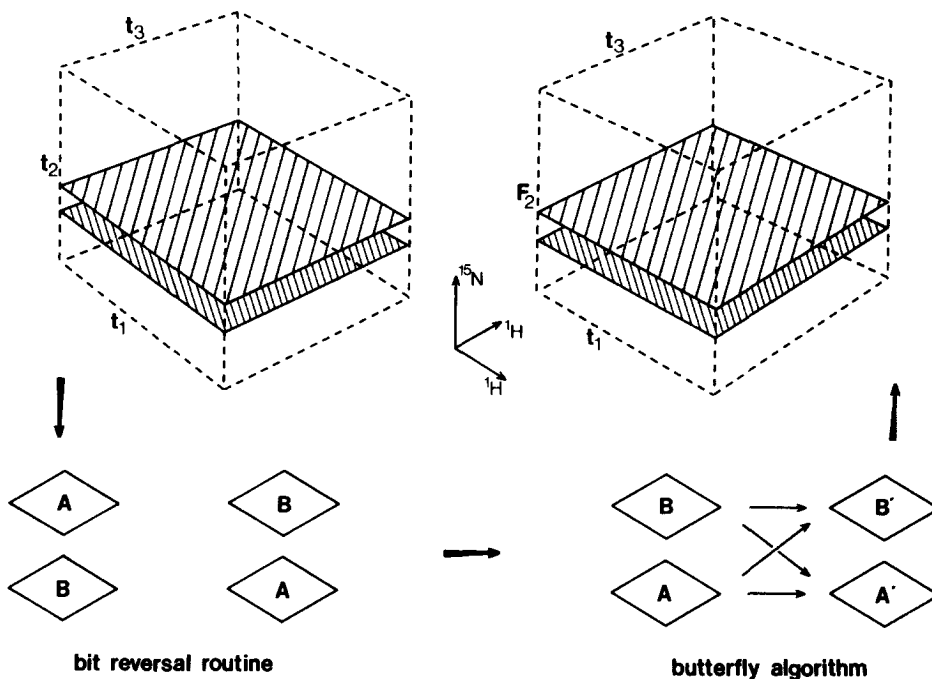
FIG. 4. Schematic representation of the Fourier transform process in t_2. Each (t_1, t_3) NOESY plane is manipulated according to the prescription for each point in a 1D transform. The transform is divided into two sections. The first consists of a bit reversal routine whereby the planes are renamed appropriately. The planes are then recombined according to the "butterfly algorithm" (27) to generate a (t_1, F_2, t_3) data set.

by the same delay. In the sequence depicted in Fig. 1, the first value of t_2 is effectively equal to $T = \tau_{180^\circ}(^1H) + (4/\pi)\tau_{90^\circ}(^{15}N) + t_2(0)$, where $t_2(0)$ is twice the value of the initial delay between the end of the 90° ^{15}N pulse and the beginning of the 180° ^1H pulse. Therefore, a linear phase shift correction across the spectrum of $(T/\Delta t_2)$ $\times$ 360° is required in F_2 (28), where Δt_2 is the dwell time in the t_2 dimension. A zero-order phase correction must be applied in order to ensure that the phase at the center of the spectrum is zero. In a similar fashion, a linear phase correction of $(T'/\Delta t_1)$ $\times$ 360°, with $T' = (4/\pi)\tau_{90^\circ}(^1H) + t_1(0)$, is required in F_1, where Δt_1 is the dwell time in t_1 and $t_1(0)$ is the initial value of the delay between the first two 90° ^1H pulses. In our experience, the calculated phase parameters are at least as accurate as phase parameters obtained manually. At this stage of the process, the imaginary data in F_2 can be discarded, reducing the size of the data matrix to the size it had before zero-filling in t_2. In the case of data acquired in the complex mode in t_1, an additional linear phase correction of the t_1 time-domain data is applied to shift the carrier position to unfold the spectrum, as discussed above. Since the parameters for both the phasing and the unfolding processes can be calculated without visual inspection of any of the Fourier-transformed spectra, all of the processes described in Fig. 3 can be executed automatically. On the SUN-4-110 system used for data processing, a $(2 \times 128) \times (2 \times 32) \times (2 \times 256)(t_1, t_2, t_3)$ matrix consisting of single precision floating point data requires approximately 1.5 hours to reach this stage of processing. As the

diagram in Fig. 3 indicates, existing commercial software is used to process the 2D NOESY planes which are then stored as separate 2D files on disk.

Several points pertaining to the software that we have developed deserve attention. First, it is not necessary to do the initial processing of the data in the dimension in which it is acquired (F_3 in this case, F_2 in the case of 2D experiments). Having the flexibility of processing the data in another dimension first may have certain advantages for both 3D and 2D experiments. For example, for the 3D experiment of Fig. 1, processing of the data in t_2 generates a set of standard NOESY spectra. If particular NOE information is required it is not necessary to process all the data; the pertinent information can simply be extracted from a single (t_1, t_3) slice, taken at the appropriate ^{15}N chemical shift. Extensive zero-filling may then be used for this relatively small 2D matrix. A second advantage lies in the fact that for a 2D spectrum the F_1 phasing parameters and for a 3D spectrum both the F_1 and the F_2 phasing parameters can be calculated exactly. Obtaining the exact phasing is sometimes more difficult in F_3, in particular if one must use a t_3 slice through the (t_1, t_2, t_3) time-domain data, where a single FID typically yields a spectrum with a poor signal-to-noise ratio. In the case of 2D NMR data similar problems with phasing in F_2 exist. Most existing 2D software packages either save real and imaginary data in both dimensions, which requires substantial storage capabilities, or require that processing be first carried out in F_2 followed by discarding of the imaginaries. In the latter case, it is not possible to rephase the data in F_2 once the imaginaries are discarded. By processing the data first in the F_1 dimension using the calculated phasing parameters and discarding the imaginaries, followed by processing of the data in F_2, it is possible to rephase in this dimension several times if necessary. Our approach for processing of 3D data does not require the use of a time-consuming data transposition, and moreover, commercial software can be used to process the two "standard" dimensions of the 3D data set after the third dimension is processed. All modules are written in the C programming language and have been implemented on a SUN 4 computer. They are available upon request.

Figure 5 presents two NOESY slices taken from a crowded region of the 3D spectrum at ^{15}N chemical shifts of 116.8 and 118.2 ppm. The 3D spectrum was recorded in 2.5 days on a NT-500 spectrometer, on a 1.8 mM solution of S. Nase complexed with pdTp and Ca^{2+}, in 90% H$_2$O/10% D$_2$O at pH 7.5, 35°C. The sensitivity of the 3D spectrum is similar to that of the conventional NOESY spectrum (data not shown), but the severe overlap of cross peaks that is present in the 2D spectrum is almost completely removed.

The heteronuclear 3D experiment described above generates absorptive 3D spectra that have in-phase multiplets. This is particularly important for applications to large molecules where short T_2 values and signal overlap often cause extensive cancellations of antiphase signals (*29*). During the HMQC portion of the 3D experiment, favorable multiple-quantum T_2 relaxation rates are operative, due to the fact that to first order the ^{1}H–^{15}N dipolar interaction does not contribute to the relaxation process (*30*). This may be particularly important for proteins significantly larger than S. Nase, where T_2's rather than digitization will determine spectral resolution. Moreover, heteronuclear 3D experiments have the advantage that the flow of magnetization can be restricted without the need for selective pulses (*2*). For proteins significantly larger than about 10 kDa, techniques relying on the ^{1}H–^{1}H J coupling such as
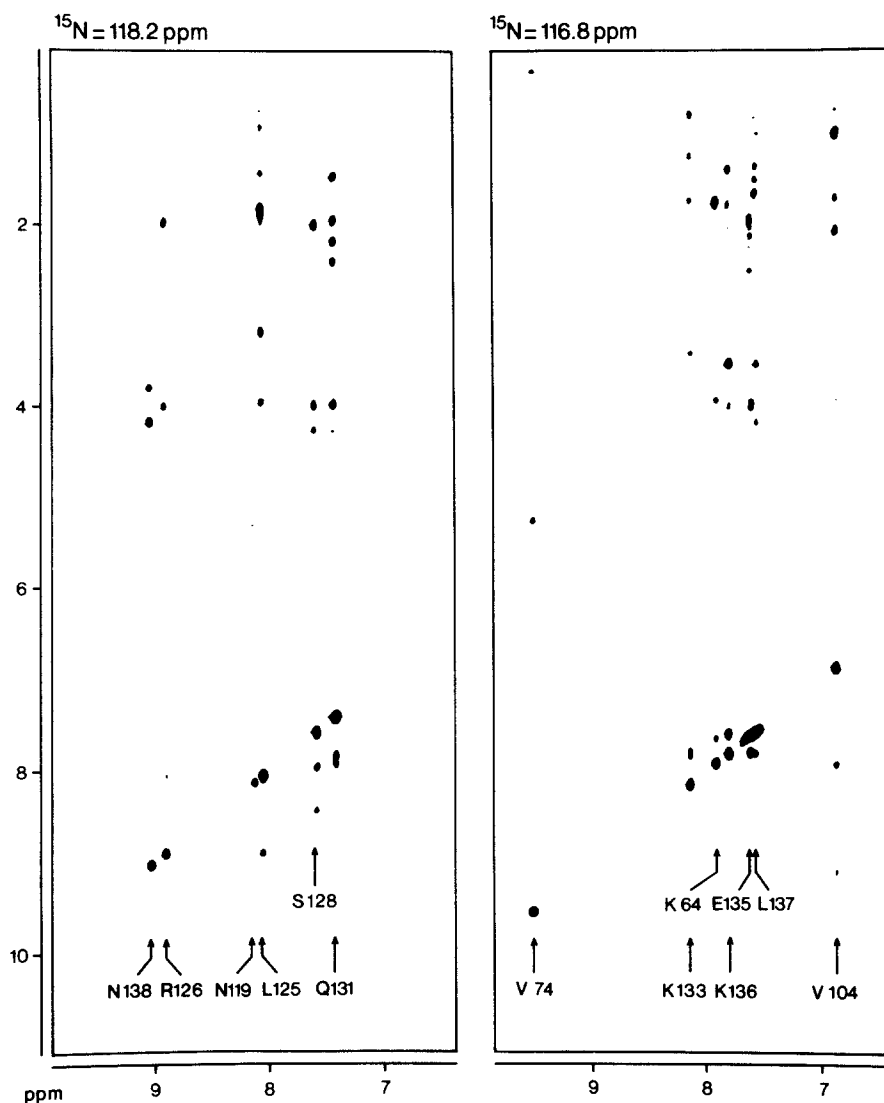
FIG. 5. F_1/F_3 slices at ^{15}N chemical shifts of 116.8 and 118.2 ppm recorded with the scheme of Fig. 1, for an NOE mixing time of 125 ms. The spectrum results from a $128 \times 32 \times 256$ complex data matrix, with acquisition times of 23, 21, and 64 ms in the t_1, t_2, and t_3 dimensions, respectively. The total measuring time was 2.5 days. Zero-filling was used in all three dimensions to yield a $256 \times 64 \times 512$ matrix for the absorptive part of the 3D spectrum. Note that in the NH–NH region of the spectra the cross peaks are asymmetrically distributed about the diagonal. Only in cases where the ^{15}N chemical shifts of both amide nitrogens overlap in the F_2 dimension (e.g., L125 and R126 in the left panel) will cross peaks be symmetrically positioned about the diagonal.

COSY and HOHAHA/TOCSY rapidly become less efficient. However, preliminary results obtained with the HOHAHA-HMQC 3D experiment for two different proteins in the range 16–18 kDa indicate that this experiment also is capable of generating high-quality spectra for proteins in this molecular weight range. Based on our

experience with 2D HOHAHA experiments, it is expected that for proteins larger than about 20 kDa the sensitivity of the HOHAHA-HMQC 3D experiment will become too low for practical use. In contrast, the NOE experiment still works very well for many of these proteins and we therefore believe that the NOESY-HMQC experiment will be applicable to proteins significantly larger than 20 kDa.

<div align="center">APPENDIX</div>

This appendix provides a theoretical description of the effects of the off-resonance water presaturation sequence used in the pulse scheme of Fig. 1. First will be considered the excitation versus frequency profile of a rectangular pulse. Its frequency profile can be calculated explicitly from the transient solutions of the Bloch equations (31). For a pulse of length, t_p, and of magnitude B_1, an absorption-mode component is obtained which has a dependence on the resonance offset, $\gamma \Delta B$, given by

$$A(\nu) = (B_1/B_{\text{eff}})\sin(\gamma B_{\text{eff}} t_p) \qquad [A1]$$

and a dispersion-mode signal,

$$D(\nu) = (B_1 \Delta B/B_{\text{eff}}^2)[1 - \cos(\gamma B_{\text{eff}} t_p)], \qquad [A2]$$

where $B_{\text{eff}}^2 = B_1^2 + (\Delta B)^2$ and $\nu = \gamma(\Delta B)/2\pi$.

An *approximate* excitation spectrum of a square pulse can be obtained by Fourier analysis, yielding

$$A'(\nu) = (B_1/\Delta B)\sin(\gamma \Delta B t_p) \qquad [A3]$$

and

$$D'(\nu) = (B_1/\Delta B)[1 - \cos(\gamma \Delta B t_p)]. \qquad [A4]$$

Comparing Eqs. [A1] and [A2] with Eqs. [A3] and [A4] indicates that in the limit $\Delta B \gg B_1$, Fourier analysis of a square pulse gives the correct frequency response. Moreover, it is also easily verified that in this limit the magnitude of the frequency distribution, $M(\nu) = [A(\nu)^2 + D(\nu)^2]^{1/2}$, obtained by the solution of the Bloch equations is the same as that obtained by Fourier analysis. It follows that the magnitude of the frequency distribution of any pulse train can be evaluated correctly by Fourier analysis as long as $\Delta B \gg B_1$.

The off-resonance water suppression sequence considered in this appendix is of the form $(\theta_0 \theta_\phi \theta_{2\phi} \theta_{3\phi} \cdots \theta_{(k-1)\phi})_n$, where $e^{ik\phi} = 1$ and where the duration of each θ pulse, D, is set to $1/(k\delta_{\text{H}_2\text{O}})$. In the sequence used for presaturation in Fig. 1, $\phi = \pi/2$ and $k = 4$.

In order to evaluate the magnitude of the frequency distribution, $M_{\text{WS}}(\nu)$, of the sequence $(\theta_0 \theta_\phi \theta_{2\phi} \theta_{3\phi} \cdots \theta_{(k-1)\phi})_n$, $n \rightarrow \infty$, this sequence is rewritten as

$$\sum_{m=-\infty}^{\infty} (\theta_0 \theta_\phi \theta_{2\phi} \theta_{3\phi} \cdots \theta_{(k-1)\phi})_n \circledast \delta(t - mkD)$$

$$= F(\theta) \circledast \sum_{m=-\infty}^{\infty} \delta(t - mkD) = A(t), \qquad [A5]$$

where δ is a dirac delta function defined as

$$\delta(t - mkD) = 0 \quad \text{if} \quad t \neq mkD$$

$$= 1 \quad \text{if} \quad t = mkD, \qquad [A6]$$

$F(\theta) = (\theta_0 \theta_\phi \theta_{2\phi} \theta_{3\phi} \cdots \theta_{(k-1)\phi})_n$, and $\circledast$ is the convolution operator (32). The Fourier transform of $A(t)$ gives

$$FT[A(t)] = FT[F(\theta)]/(kD) \sum_{m=-\infty}^{\infty} \delta[\nu - m/(kD)], \qquad [A7]$$

where $FT(F(\theta))$ is the Fourier transform of $F(\theta)$.

In the derivation of Eq. [A7] we have made use of the fact that the Fourier transform of the convolution of two functions is the product of their Fourier transforms (32) and that

$$FT\left[\sum_{m=-\infty}^{\infty} \delta(t - mkD)\right] = 1/(kD) \sum_{m=-\infty}^{\infty} \delta[\nu - m/(kD)]. \qquad [A8]$$

The expression for $M_{WS}(\nu)$ is given by

$$M_{WS}(\nu) = \{FT[F(\theta)]FT[F(\theta)]^*\}/(kD) \sum_{m=-\infty}^{\infty} \delta[\nu - m/(kD)], \qquad [A9]$$

where $FT[F(\theta)]^*$ is the complex conjugate of $FT[F(\theta)]$. Equation [A9] can be readily evaluated to give

$$M_{WS}(\nu) = \sum_{m=-\infty}^{\infty} |(B_1/\pi m)\sin(\omega_m D/2)|$$

$$\times \left\{ k + 2 \sum_{p=1}^{k-1} (k - p)\cos[p(\omega D + \phi)]\right\}^{1/2} \delta[\nu - \omega_m/(2\pi)], \quad [A10]$$

where $\omega_m = 2\pi m/(kD)$. For the values of ϕ and k used, $\phi = \pi/2$ and $k = 4$, Eq. [A10] reduces to a series of sidebands, centered $1/(4D)$ Hz upfield from the carrier and spaced $1/D$ Hz apart with intensities that decrease asymmetrically with respect to offset from the central band. In particular, the intensity of the B_1 field associated with the mth sideband upfield from the carrier is given by

$$B_{1_{\text{eff}}}(m) = 2\sqrt{2}B_1/[\pi(4m - 3)], \qquad [A11]$$

while the intensity of the B_1 field associated with the mth sideband downfield of the carrier is given by

$$B_{1_{\text{eff}}}(m) = 2\sqrt{2}B_1/[\pi(4m - 1)]. \qquad [A12]$$

The carrier frequency is chosen such that only the central band lies within the spectrum. In the applications of this sequence, typically $\gamma B_1/2\pi \approx 10\text{–}15$ Hz and the carrier is positioned 2000 Hz from the water resonance so that $\gamma \Delta B/2\pi = 2000$ Hz. Therefore the condition that $\Delta B \gg B_1$, which is required for Eq. [A10] to be valid, is satisfied. Equation [A10] has been derived in the limit as $n \rightarrow \infty$. For finite values of n, Eq. [A10] must be convoluted with a sinc function which has a width of $2/t_d$

between the first zero-crossing points, where t_d is the duration of the pulse train (31). For typical values of t_d ($1-2$ s), this additional factor has no significant effect and can be neglected.

ACKNOWLEDGMENTS

REFERENCES

1. H. D. PLANT, T. H. MARECI, M. D. COCKMAN, AND W. S. BREY, "27th ENC Conference," Poster A23, Baltimore, Maryland, 1986.
2. C. GRIESINGER, O. W. SØRENSEN, AND R. R. ERNST, J. Magn. Reson. 73, S74 (1987).
3. C. GRIESINGER, O. W. SØRENSEN, AND R. R. ERNST, J. Am. Chem. Soc. 109, 7227 (1987).
4. G. W. VUISTER AND R. BOELENS, J. Magn. Reson. 73, 328 (1987).
5. H. OSCHKINAT, C. GRIESINGER, P. J. KRAULIS, O. W. SØRENSEN, R. R. ERNST, A. M. GRONENBORN, AND G. M. CLORE, Nature (London) 332, 374 (1988).
6. S. W. FESIK AND E. P. R. ZUIDERWEG, J. Magn. Reson. 78, 588 (1988).
7. G. W. VUISTER, R. BOELENS, AND R. KAPTEIN, J. Magn. Reson. 80, 176 (1988).
8. D. MARION, L. E. KAY, S. W. SPARKS, D. A. TORCHIA, AND A. BAX, J. Am. Chem. Soc. 111, 1515 (1989).
9. J. JEENER, B. H. MEIER, P. BACHMANN, AND R. R. ERNST, J. Chem. Phys. 71, 4546 (1979).
10. S. MACURA AND R. R. ERNST, Mol. Phys. 41, 95 (1980).
11. L. BRAUNSCHWEILER AND R. R. ERNST, J. Magn. Reson. 53, 521 (1983).
12. A. BAX AND D. G. DAVIS, J. Magn. Reson. 65, 355 (1985).
13. W. P. AUE, E. BARTHOLDI, AND R. R. ERNST, J. Chem. Phys. 64, 2229 (1976).
14. A. BAX AND R. FREEMAN, J. Magn. Reson. 44, 542 (1981).
15. K. NAGAYAMA, A. KUMAR, K. WÜTHRICH, AND R. R. ERNST, J. Magn. Reson. 40, 321 (1980).
16. L. P. MCINTOSH, R. H. GRIFFEY, D. C. MUCHMORE, C. P. NIELSON, A. G. REDFIELD, AND F. W. DAHLQUIST, Proc. Natl. Acad. Sci. USA 84, 1244 (1987).
17. M. A. WEISS, A. JEITLER-NILLSON, N. J. FISCHBEIN, M. KARPLUS, AND R. T. SAUER, in "NMR in the Life Sciences" (E. M. Bradbury and C. Nicolini, Eds.), pp. 37–48, NATO ASI Series, Vol. 107, Plenum, London, 1986.
18. J. JEENER, B. H. MEIER, P. BACHMANN, AND R. R. ERNST, J. Chem. Phys. 71, 4546 (1979).
19. E. R. P. ZUIDERWEG, K. HALLENGA, AND E. T. OLEJNICZAK, J. Magn. Reson. 70, 336 (1986).
20. A. BAX, R. H. GRIFFEY, AND B. L. HAWKINS, J. Magn. Reson. 55, 301 (1983).
21. M. R. BENDELL, D. T. PEGG, AND D. M. DODDRELL, J. Magn. Reson. 52, 81 (1983).
22. M. H. LEVITT, G. BODENHAUSEN, AND R. R. ERNST, J. Magn. Reson. 58, 462 (1984).
23. D. MARION AND K. WÜTHRICH, Biochem. Biophys. Res. Commun. 113, 967 (1983).
24. D. J. STATES, R. A. HABERKORN, AND D. J. RUBEN, J. Magn. Reson. 48, 286 (1982).
25. A. A. BOTHNER-BY AND J. DADOK, J. Magn. Reson. 72, 540 (1987).
26. R. R. ERNST, G. BODENHAUSEN, AND A. WOKAUN, "Principles of Nuclear Magnetic Resonance in One and Two Dimensions," Clarendon, Oxford, 1987.
27. W. H. PRESS, B. P. FLANNERY, S. A. TEUKOLSKY, AND W. T. VETTERLING, "Numerical Recipes, The Art of Scientific Computing," Cambridge Univ. Press, London/New York, 1986.
28. A. BAX AND D. MARION, J. Magn. Reson. 78, 186 (1988).
29. K. WÜTHRICH, "NMR of Proteins and Nucleic Acids," Wiley, New York, 1986.
30. A. BAX, L. E. KAY, S. W. SPARKS, AND D. A. TORCHIA, J. Am. Chem. Soc., in press.
31. A. G. MORRIS AND R. FREEMAN, J. Magn. Reson. 29, 433 (1978).
32. R. M. BRACEWELL, "The Fourier Transform and Its Applications," McGraw–Hill, New York, 1965.